RECONSTRUCTION OF PHOTON ENERGY SPECTRA FROM CLINICAL PERCENTAGE DEPTH-DOSE CURVES USING TIKHONOV REGULARIZATION AND GENERALIZED SIMULATED ANNEALING

RECONSTRUCCIÓN DEL ESPECTRO DE ENERGÍA DE FOTONES A PARTIR DE CURVAS CLÍNICAS DE DOSIS PORCENTUAL EN PROFUNDIDAD MEDIANTE REGULARIZACIÓN DE TIKHONOV Y GENERALIZED SIMULATED ANNEALING

Jorge H. Wilches Visbal[1], Giulianne R. Rodrigues Zaratim[2], Ana Quevedo[3], Luciana Cardoso Matsushima[4], Glauco Rogério Veneziani[5], Iury Mergen Knoll[6], Alexandre Bonatto[6,7] and Mirko Alva Sánchez[6,7*]

[1] School of Health Sciences, University of Magdalena. Lab of Biophysics, Innovation and Entrepreneurship Building, Colombia.
[2] Faculdade UnB Gama - FGA, Universidade de Brasília, Brazil.
[3] Department Health Science, Oeste Paulista University – UNOESTE, Brazil.
[4] Instituto de Física da Universidade Federal de Goiás- Campus Samambaia, Brazil.
[5] Dosemed Soluções em radioterapia, Brazil.
[6] Graduate Program in Information Technologies and Health Management, Federal University of Health Sciences of Porto Alegre-UFCSPA, Brazil.
[7] Beam Physics Group, Federal University of Health Sciences of Porto Alegre – UFCSP, Brazil.

(Received: Apr./2025. Accepted: Oct./2025)

Abstract

The primary objective of this study is to reconstruct the energy spectrum from three linear accelerators (LINACs) using experimental measurements of the percentage depth dose (PDD) curve. The experimentally obtained percentage depth dose curves were used to solve the Fredholm integral equation. The photon beam spectra are related to radiation doses through a Fredholm integral equation, utilizing the generalized simulated annealing optimization method.

* mirko@ufcspa.edu.br doi: https://doi.org./10.15446/mo.n72.119862

The resulting spectrum was used to simulate an irradiation reference condition as recommended by TRS-398. The Monte Carlo codes PENELOPE and TOPAS were employed to create the simulation scenario under reference conditions (10 x 10 cm^2 field size, 100 cm SSD, and 30 x 30 x 30 cm^3 water phantom) for 6 MeV photon beams. The calculated spectra from the three LINACs demonstrated a remarkable level of concordance, achieving up to 99% agreement.

The validation of the reconstructed spectrum was carried out by comparing it with the PDD and beam profile curves, revealing a highly favorable correspondence in their behavior. A comprehensive analysis compared the experimentally acquired PDDs with those simulated using the reconstructed spectrum. Parameters such as the entrance dose and $TPR_{20/10}$ were derived from the PDD curves for evaluation. Upon conducting a thorough comparison of these parameters with the experimental dataset, noticeable deviations of 10% (entrance dose), and 3% ($TPR_{20/10}$). Beam profile comparisons across field size dimensions revealed differences ranging from 0.5% to 5.3%. The present study encompassed the reconstruction of the photon beam spectrum originating from LINACs, revealing a noteworthy level of agreement among them. The validation of the Fredholm integral equation by utilizing

two simulation codes, as facilitated by the analysis of the PDD and beam profile curves, revealed substantial disparities within the region leading up to the build-up point. This reconstructed spectrum holds considerable potential for simulation scenarios within radiotherapy applications. This significance is particularly underscored by the challenges associated with acquiring comprehensive data from manufacturers of LINACs, which impedes access to crucial information regarding the constituents of these accelerators.

Keywords: spectral reconstruction, photon beams, radiotherapy, Monte Carlo simulation.

Resumen

El objetivo principal de este estudio es reconstruir el espectro de energía de tres aceleradores lineales (LINACs) utilizando mediciones experimentales de la curva de dosis en profundidad porcentual (PDD). Las curvas del porcentaje de dosis en profundidad obtenidas experimentalmente se utilizaron para resolver la ecuación integral de Fredholm. Los espectros de los haces de fotones están relacionados con las dosis de radiación a través de una ecuación integral de Fredholm, utilizando el método de optimización de recocido simulado generalizado. El espectro resultante se empleó para simular una condición de irradiación de referencia según lo recomendado por el TRS-398. Los códigos de Monte Carlo PENELOPE y TOPAS se utilizaron para crear el escenario de simulación en condiciones de referencia (tamaño de campo de 10 x 10 cm^2, SSD de 100 cm y un fantoma de agua de 30 x 30 x 30 cm^3) para haces de fotones de 6 MeV. Los espectros calculados de los tres LINACs demostraron un notable nivel de concordancia, alcanzando hasta un 99% de acuerdo. La validación del espectro reconstruido se llevó a cabo comparándolo con las curvas de PDD y los perfiles del haz, revelando una correspondencia altamente favorable en su comportamiento. Se realizó un análisis comparativo entre las PDD adquiridas experimentalmente y aquellas simuladas con el espectro reconstruido. Se derivaron parámetros como la dosis de entrada y el $TPR_{20/10}$ a partir de las curvas de PDD para su evaluación. Al comparar estos parámetros con los datos experimentales, se observaron desviaciones notables del 10% (dosis de entrada) y del 3% ($TPR_{20/10}$). Las comparaciones de perfiles del haz en diferentes tamaños de campo revelaron diferencias que oscilaron entre el 0.5% y el 5.3%. Este estudio abarcó la reconstrucción del espectro del haz de fotones originado en LINACs, mostrando un nivel significativo de concordancia entre ellos. La validación de la ecuación integral de Fredholm mediante la utilización de dos códigos de simulación, a través del análisis de las curvas de PDD y del perfil del haz, reveló discrepancias sustanciales en la región build-up. El espectro reconstruido tiene un

considerable potencial para la simulación de escenarios en aplicaciones de radioterapia. Esta relevancia se ve particularmente resaltada por los desafíos asociados con la obtención de datos detallados de los fabricantes de LINACs, lo que dificulta el acceso a información crucial sobre los componentes de estos aceleradores.

Palabras clave: reconstrucción espectral, haces de fotones, radioterapia, simulación de Monte Carlo.

Introduction

Clinical beams, including photons and electrons, are widely used in radiotherapy [1, 2]. Maintaining an uncertainty range of -5% to +7% between prescribed and delivered doses, as recommended by the ICRU, is a continuous challenge [3]. Dosimetric parameters like PDD are crucial for accurate dose measurement. Experimental measurements with dosimeters can provide the determination of dosimetric parameters, essential for treatment planning and quality control [4].

The Monte Carlo method is useful for determining dosimetric parameters, especially for difficult-to-measure physical properties [5, 6]. Codes like GATE [7], MCNP [8, 9], PENELOPE [10, 11], and TOPAS [12, 13] and others have been simulated radiation transport under various irradiation conditions and geometries.

PENELOPE, a Monte Carlo-based FORTRAN code, simulate the radiation transport from linear accelerator heads, encompassing all components and external spectra with specific field sizes [14, 15], also as TOPAS, another Monte Carlo tool, simplifies advanced radiotherapy simulations without requiring expertise in the Geant4 Simulation Toolkit or programming [16, 17]. This accessibility makes TOPAS valuable for researchers and practitioners in radiation therapy.

These codes model interactions within the LINAC head, such as with the primary collimator, ionization chamber, and secondary

collimators. They can simulate energy spectra from virtual focal points [18–20].

Energy spectra from a LINAC can be reconstructed using mathematical models. Traditional linearization methods can be error-prone, requiring alternative algorithms. From a different standpoint, various alternative methods have been proposed, each with its distinct limitations. For instance, certain approaches exhibit constraints tied to the experimental apparatus's geometry. These methods tend to overlook crucial geometric parameters, regardless of the type and shape of the dimensioned filter being used. An illustrative instance is the study conducted by Jalbout and collaborators, where the Schiff formula and dispersion analysis were employed for reconstruction. However, this approach introduced limitations related to experimental geometry [21].

Studies reconstruct spectra from clinical beams using analytical and simulation techniques, addressing the challenges of high-energy beam measurement [9]. Deng et al. found substantial agreement between reconstructed and actual spectra from a Varian linear accelerator [22]. Manrique used Compton scattering to reconstruct spectra from a Co-60 teletherapy machine [23].

Additionally, several studies have employed neural networks to address specific linear equation conditions, using percentage depth dose curves as well [24]. Photon beam transmission measurements, combined with the response of an ionization chamber, have also been used [25]. Another approach utilizes an in-house Monte Carlo (MC) algorithm, as demonstrated by Can et al. (2022). Furthermore, a separate study proposed a source model for a 6 MeV LINAC both with and without a flattening filter [26].

This study aimed to reconstruct the spectrum of a megavoltage photon beam using Tikhonov regularization and the Fredholm integral equation of the first kind. The spectra were validated using PDD and beam profile curves from the two simulation codes PENELOPE and TOPAS. They can be a valuable complementary tool for routine radiotherapy dosimetry and quality control.

Materials and methods

Mathematical modeling of the inverse reconstruction

By utilizing the Fredholm integral equation of the first kind, it becomes possible to establish a relation between the central-axis energy spectrum of a megavoltage photon beam, denoted as $\varphi_E(E)$, and the measured percentage depth-dose, denoted as D_z, which pertains to the region reaching the surface of the phantom [27–30].

$$D_z(z) = \int_{E_{\min}}^{E_{\max}} D(z,E)\varphi_E(E)\,dE, \tag{1}$$

where $D(z,E)$ is a matrix of monoenergetic PDDs simulated using Monte Carlo methods (or obtained through analytical techniques). These PDDs are derived from beams with nominal energies ranging between $E_{\min}$ and $E_{\max}$, divided into intervals of dE. In simpler terms, $D(z,E) = [\mathrm{PDP}_{E_{\min}}, \mathrm{PDP}_{E_{(\min+dE)}}, \mathrm{PDP}_{E_{\min+2dE}}, \ldots, \mathrm{PDP}_{E_{\max}}]$ with z being the depth of clinical measurement in the phantom.

Since it is impossible to obtain $D(z,E)$ with $dE \to 0$, the Eq. (1) must be discretized in a way that,

$$D_z \cong \sum_{i,j}^{m,n} D(z_i,E_j)\varphi_{E_j}(E_j)\Delta E_j, \tag{2}$$

where $i = \ldots[1,2,3,..,m]$ is the i-th depth of dose measurement bin, $j = \ldots[1,2,3,..,n]$ is the j-th monoenergetic photon beam and ΔE_j is the energy interval between two consecutive monoenergetic beams. So, D_z is a $m \times 1$ vector, $D(z_i,E_j)$ is a $m \times n$ matrix and $\varphi_{E_j}(E_j)$ a $1 \times n$ vector.

Thereby, Eq. (2) may be rewritten as a linear system of equations, such that,

$$D_z = D(z,E)\Delta E\varphi(E), \tag{3}$$

with $D(z,E)\Delta E$ is named as the kernel of equation, $K(z,E)$,

$$D_z = K(z,E)\varphi(E). \tag{4}$$

The inverse matrix (IM) or least squares methods (LSQM) could be utilized to solve Eq. (4) in order to extract the photon spectrum [30]. However, as extracting $\varphi_E(E)$ from $D_z(z)$ in Eq. (4) represents an inverse problem (usually ill-posed) [31], IM and LSQM fail in finding a useful and stable solution. The reason of this is that Eq. (1) is inherently ill-posed [31, 32], i.e., small perturbations in entrance data produce big errors in the output [33]. Therefore, the derivation of $\varphi(E)$ from D_z, by applying Eq. (4), requires the use of some regularization technique [29, 33].

Regularization Method

One of the most widely used regularization methods for addressing ill-posed problems is Tikhonov regularization. It involves the filtration of perturbations in the input data to achieve a solution that: i) closely aligns with the desired outcome (low bias); ii) remains minimally affected by noise in the input data (low variance); and iii) represents an optimal balance between bias and variance.

Tikhonov regularization, which was developed by Tikhonov and Phillips in the 1960s, finds utility in solving Fredholm equations of the first kind [27, 32, 34].

In mathematical terms, Tikhonov regularization involves minimizing the functional $\mu(\varphi)$, which is composed of the sum of solution and residual semi-norms, as expressed below [35],

$$\mu(\varphi) = \|K(z,E)\varphi(E) - D_z\|_2^2 + \lambda^2 \|L(\varphi(E) - \varphi_0(E))\|_2^2, \tag{5}$$

where L is the regularization matrix and λ is the regularization parameter. L is a derivative operator's matrix and φ_0 is the initial

solution attempt [27]. The initial solution was built from a priori information about the unknown [36] (Figure 1).

In Eq. (5), λ controls the degree of smoothing (or regularization) on the sought solution. A high value of λ leads to a smooth solution at the expense of decreasing its accuracy (distance between the estimated and real solution). In contrast, a low value of λ may lead to a solution close to the real although noisier. For this reason, λ must be carefully selected [35].

The regularization parameter λ was initially estimated from the L-curve and refined using the GSA optimizer following Wilches et al. (2020). The selected value $\lambda = 1.65$ represents the inflection point of the curve, balancing the residual and constraint norms. Sensitivity analysis ($\Delta\lambda = \pm 0.1$) showed variations below 0.4% in spectral parameters and γ-passing $> 95\%$ (1%/1 mm).

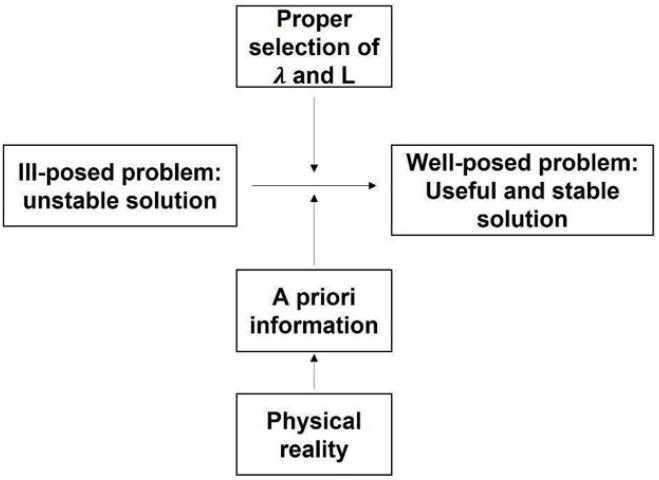

FIGURE 1. *Solution of an ill-posed problem by Tikhonov regularization*

In this context, suitable solutions are achieved when L represents a first-order derivative matrix [27, 29]. While the L-curve method can be employed to determine λ [37], the optimal parameter value is likely derived through trial and error, tailored to each specific scenario [36]. The regularization matrix and parameter can be computed using the regularization package developed by Hansen

[35]. To minimize $\mu(\varphi)$, employing an optimization method is highly recommended.

Optimization Method

An optimization method involves determining the global minimum or maximum of an objective function (functional) associated with a specific problem. Optimization methods can be categorized as stochastic or deterministic. Deterministic methods consistently yield the same output given identical inputs. Conversely, methods that do not follow this pattern are labeled stochastic. This approach offers the notable advantage of circumventing confinement to local optima and aiming for the global optimum. However, a drawback is that stochastic methods are often slower compared to their deterministic counterparts [38].

Among the most dependable and extensively used optimization methods for seeking the global optimum of multidimensional functions is generalized simulated annealing (GSA). The concept of GSA is inspired by the process of simulated annealing in metallurgy, where a metal is gradually heated to its fusion temperature and then cooled meticulously to attain a defect-free crystalline structure [39].

In 2019, one of the authors developed a MATLAB function based on GSA, which is comprehensively detailed in Wilches-Visbal et al. (2022) and Wilches and Da Costa, (2019). This function has been effectively employed for the reconstruction of clinical electron [27, 29] and kilovoltage photon beam spectra [40].

The minimization of the Tikhonov functional was carried out using the Generalized Simulated Annealing (GSA) algorithm described in Wilches & Da Costa (2019, Ingeniería y Ciencia). GSA modifies the conventional simulated annealing through non-extensive statistics, enabling a power-law visiting distribution that ensures global convergence. The parameters $qv = 2.7$, $qa = -5.0$ and $T_{\max} = 1000$ were used as previously validated. Compared with deterministic least-squares optimization, GSA avoids local minima and is more robust for noisy and ill-posed inverse problems.

Implementation and validation of the spectral reconstruction process

The process of deriving energy spectra for megavoltage photon beams from PDD curves is delineated in the subsequent steps:

1. To obtain the percentage depth dose, $D_z(z)$, the proposed algorithm utilized the clinical PDD, acquired through measurements in a water phantom ($30 \times 30 \times 30$ cm^3) subjected to irradiation by 6 MeV nominal energy photon beams emitted from three distinct Varian Clinac CX linear accelerators (Varian Medical Systems, Palo Alto, CA, USA). These PDD curves were provided by three prominent reference hospitals in Brazil. All measurements were conducted employing the ionization chamber 31010 semiflex PTW, boasting a sensitive volume of 0.125 cm^2.

2. Construction of the kernel of depth-doses function $K(z, E)$. The kernel was built by adding, in columns, PDD curves of photon beams of nominal energies 0.125, 0.25, 0.375, ..., 6 MeV. Measurement depths range from 0.2 to 29.8 cm, with 0.2 cm interval; $K(z, E) = [\mathrm{PDP}_{(0.125\ \mathrm{MeV})}, \mathrm{PDP}_{(0.25\ \mathrm{MeV})}, \mathrm{PDP}_{(0.375\ \mathrm{MeV})}, \ldots, \mathrm{PDP}_{(6\ \mathrm{MeV})}]_{(158\times48)} \times 0.125$ MeV. The irradiation was conducted with a 2.86° angular aperture by employing the SPYRAM function of PENELOPE 2008 [10], resulting in a field size of 10×10 cm^2 on the surface. A resolution of 0.199 cm/pixel was applied, with a particle count of 2×10^9. Simulations were executed using to recreate a scenario involving the irradiation of a point source positioned 100 cm above a phantom ($30 \times 30 \times 30$ cm^3). The number of simulated showers was 1.5×10^9 (EABS (1:3) = 1×10^4 keV; C1 = C2 = 0.4 and WCC = WCR = 1×10^4 keV), to guarantee a statistical uncertainty of 2% (3σ) to the maximum depth in the phantom. The Tool for Particle Simulation, TOPAS, simulation code also was employed for comparison, as it stands as a promising tool for advanced simulations using the Monte Carlo method in radiotherapy applications. What distinguishes TOPAS is its capability to facilitate such simulations without necessitating prior familiarity with the underlying Geant4 Simulation Toolkit or any programming language [16, 17]. The simulation scenario was set up with the same geometry as that employed by the PENELOPE code. Given that TOPAS is an extension of the Geant4 Simulation Toolkit code, the Geant4_Modular and g4em-penelope packages were adopted as physics lists. A resolution of 0.2 cm/pixel was achieved, and the highest uncertainty associated with dose deposition was below 1%.

3. Establishing the initial energy spectrum. This spectrum, $\varphi_0(E)$, was assumed as a ones vector, i.e., $\varphi_0 = [1; 1; 1; \ldots; 1]_{(48\times1)}$.

4. Specification of the regularization matrix, L, and the regularization parameter, λ. The regularization matrix was computed by means of get_l(n, r) function included in Hansen's regularization package, with $r = 1$ and $n = 48$. The regularization parameter was chosen by try and failure. The best result found was $\lambda = 1.65$.

5. Reconstruction of the energy spectrum, $\varphi(E)$. With the anterior data, $\mu(\varphi)$ was minimized through the GSA function of [38], considering $q_{(v)} = 2.7$, $q_{(v)} = -5$ and $I_{Imax} = 500$. This process was repeated 4 times, where φ_0 was actualized to the φ found in each cycle. The φ suffered another smoothing, each time in the loop, by the rlowess method. Lastly, the energy spectrum chosen was the last one. The calculations of the spectral reconstruction were performed with MATLAB® 2017a on a personal computer running Microsoft Windows 10 Pro 64-bit (Core: i7, CPU: 1.8 GHz, RAM: 12 Gb).

6. Validation of the spectral reconstruction. The validation of the spectral reconstruction was performed by comparing the simulated PDD, derived from the reconstructed spectrum (referred to as simulated PDD), with the experimental PDD, associated with an uncertainty of 1.8%, was provided by the company, and the data originates from a reference hospital. This comparison was conducted employing the percentage difference, as shown in Fig. 3. Furthermore, supplementary validation was undertaken using the beams' quality index, specifically the $\mathrm{TPR}_{20/10}$ [41].

$$TPR_{20/10} = 1.2661, \quad PDD_{20/10} - 0.0595, \tag{6}$$

where $\mathrm{PDD}_{20/10}$ is the quotient of the value of PDD at $z = 20$ cm with respect to the one at $z = 10$ cm, for a 10×10 cm^2 field size and 100 cm SSD. With this, $\mathrm{TPR}_{20/10}$ experimental and simulated PDD curves were compared through the percentage relative error. In addition to the PDD curves, the algorithm validation includes beam profile curves, comparing data obtained through the PENELOPE code, which uses the reconstructed spectrum, as well as the beam profiles generated by the algorithm, with those provided by the commissioning company under conditions of 10 cm depth, 10×10 cm^2 field size, and 100 cm SSD. The experimental beam profiles were provided by the commissioning company for each LINAC, using the same irradiation conditions under which the PDD curves were measured. For the Monte Carlo simulations, the dose kernel used to generate the PDD curves was applied. Consequently, the spatial distribution of the radiation dose across the central axis of a 10×10 cm^2 field, perpendicular to the dose kernel, was analyzed at a depth of 10 cm.

Results and Discussion

Reconstruction of the energy spectrum

The implementation of the algorithm, grounded in the inverse reconstruction modelling, yielded the reconstructed spectra for three distinct linear accelerators, as depicted in Fig. 2.

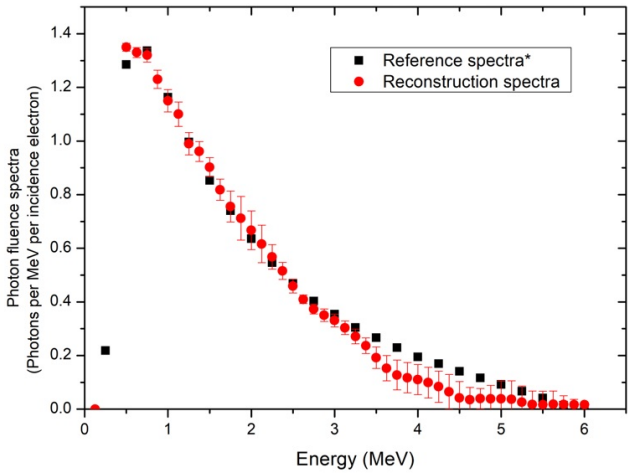

FIGURE 2. *Reconstructed spectrum of 6 MeV photon beams based on PDD measurements from three different VARIAN LINACs (model CX) and the reference spectrum [42]**

The spectrum depicted in Fig. 2 demonstrates consistent behavior, with all the curves normalized to the maximum value. The most notable disparity was 0.4% at energy levels ranging from 1.5 to 6 MeV. The errors in the reconstructed spectra are directly associated with the experimentally obtained PDDs, which had an uncertainty of 1.6%. This value was determined by propagating the errors from the dose measurements taken at various depths.

The reconstructed spectra obtained were utilized in simulations using the PENELOPE code, carried out under reference conditions as prescribed by TRS-398, for each spectrum reconstruction. The mean value of the energy spectra reconstructed in this study was compared with those obtained by Sheikh-Bagheri and Rogers (2002) [42], as shown in Fig. 2. The maximum deviation observed was 8.2% at 5.1 MeV. Additionally, a decrease in the reconstructed spectra from 1 MeV was consistent with other published works [9, 43–45]. Notably, the method used in this study showed a significant difference starting from 3.3 MeV.

Validation of the spectral reconstruction

The outcomes of the dose kernels were employed to generate PDD curves, as illustrated in Fig. 3. Moreover, utilizing the dose kernel, parameters including entrance dose, maximum dose, and the quality parameter ($TPR_{20/10}$) were derived, as presented in Equation 6.

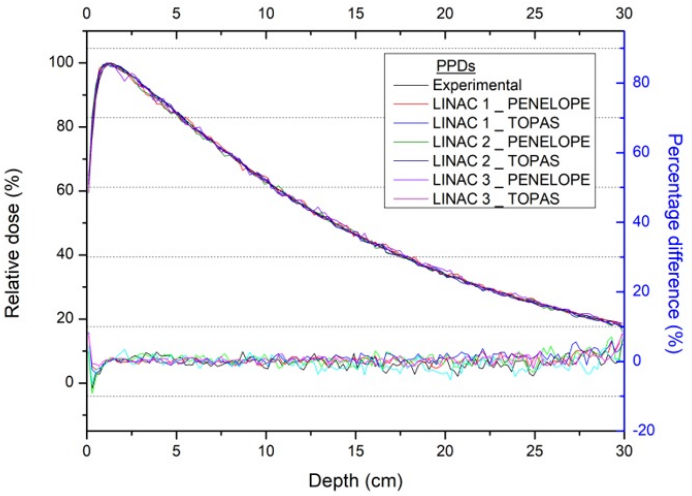

FIGURE 3. *Simulated PDDs using the reconstructed spectrum of 6 MeV photon beams, based on PDD measurements from three VARIAN LINACs (model CX)*

The PDD curves presented in Fig. 3 exhibit consistent behavior when comparing the experimental and simulated PDDs. The PDDs generated using the reconstructed spectrum were compared with two parameters: valued entrance, parameters encompassing the region up to the build-up and $TPR_{20/10}$, as detailed in Table 1.

	Entrance dose (%)			**$TPR_{20,10}$**		
	Experimental	PENELOPE	TOPAS	Experimental	PENELOPE	TOPAS
LINAC 1	65.82	63.99	59.63	0.66	0.63	0.66
LINAC 2	65.99	63.17	59.33	0.66	0.68	0.63
LINAC 3	65.81	62.99	60.40	0.66	0.65	0.64

TABLE 1. *Derived Entrance dose (at 0.2 cm) , and $TPR_{20,10}$ from PDD values, obtained through reconstructed spectrum and experimental measurements*

As indicated in Table 1, the entrance parameter of the PDDs up to the build-up region exhibited the most substantial disparity between experimental and simulation data. This was especially evident when compared to TOPAS, where the values showed approximately a 10% difference between the PDDs obtained from the three analysed linear accelerators. Compared with PENELOPE, the differences reached up to 8%, consistent with similar findings in related studies [41, 46]. Considering the sensitive volume of 0.15 cm^3 from the ionization chamber (IC) and the 0.2 cm/pixel resolution from both Monte Carlo code simulations, the difference between the entrance dose obtained with the IC and both Monte Carlo codes can be explained by the collection of more low-energy electrons from the non-electronic equilibrium region. This causes the IC to overestimate dose measurements around the entrance of the phantom [47]. These low-energy electrons originate from the interaction between the phantom and the primary photon beam [48].

It is worth noting that in the build-up region, the dose increases until reaching its maximum due to the production of secondary electrons generated by the interaction of the photon beam with the target medium. Thus, the increase in the measured dose can be attributed to secondary electrons scattered from the ionization chamber walls, which influence dose accumulation within the studied energy range and may contribute to the differences observed between the experimental data and the results obtained using the reconstructed spectrum [48, 49]. Furthermore, the beam fluence, affected by secondary photons and electrons produced in the head of a linear accelerator, can also contribute to the disparities between experimental and simulation results [41, 46].

A maximum difference of 1% was observed between simulated data and experimental PDD values, specifically for the maximum dose at a depth of 1.5 cm. Regarding the quality parameter, $TPR_{20/10}$, an analysis across the three linear accelerators revealed differences of up to 4.55% in percentage when comparing simulated data with the PDD values obtained through Monte Carlo simulation.

Results obtained using various methods to achieve the primary objective of this study have been documented. For instance, neural networks have been employed to address certain linear equation conditions, utilizing percentage depth dose curves as well [50]. Photon beam transmission measurements coupled with the response of an energy chamber have also been used [25].

Another approach involves the utilization of an in-house Monte Carlo (MC) algorithm, as demonstrated by Can et al. (2022). Furthermore, a distinct study proposed a source model for a 6 MeV LINAC with and without a flattening filter [26]. Fig. 3 presents the PDD curves obtained using the reconstruction spectrum with the PENELOPE and TOPAS Monte Carlo codes for 6 MeV

photon beams. It illustrates the percentage difference between the PDD values obtained from the simulation codes and the experimental results.

Beam profile curves obtained using the PENELOPE code, which incorporates the reconstructed spectrum, were compared with those provided by the commissioning company under conditions of 10 cm depth, a 10×10 cm^2 field size, and 100 cm SSD, as illustrated in Fig. 4.

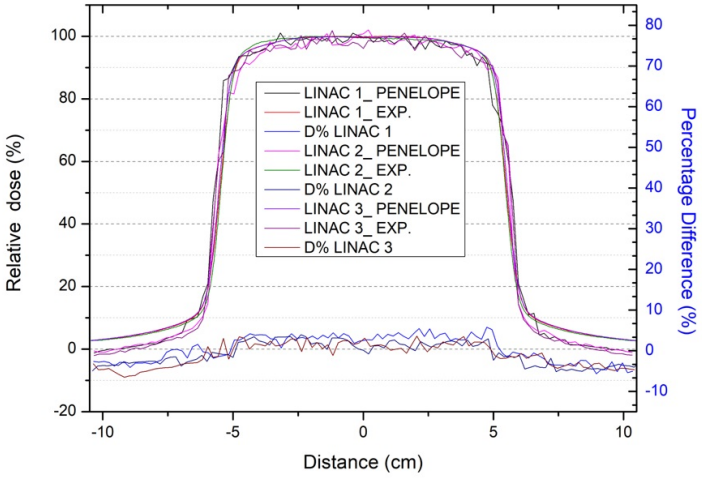

FIGURE 4. *Beam profile curves derived from experimental data compared to those obtained using the reconstructed spectrum for three different VARIAN LINAC models (CX)*

Within the 10 cm lateral field dimension, the comparison of beam profile curves revealed percentage differences ranging from 0.5% to 5.3% between the simulation data and the experimental results from the three LINAC evaluations. Significant differences were observed in the penumbra regions and beyond, with percentage differences reaching approximately 10%.

This variation may be attributed to the area defined by the jaw aperture, which delimits the required field size. Simultaneously, the penumbra is strongly influenced by the jaw edge, which generates secondary beams. Consequently, using only the reconstructed spectrum introduced variances in the beam profile, as fewer simulated particles reached the penumbra and peripheral regions outside the irradiation field, leading to substantial statistical fluctuations.

Overall, the results obtained are closely aligned with those in the field aperture region and penumbra areas, consistent with findings from other studies [51–54].

Conclusions

This study has demonstrated that reconstructing the spectrum from three LINAC through Tikhonov regularization with an automated method employing simulated annealing is a feasible approach. This validation process indicates that the obtained spectrum can be valuable for replicating scenarios in radiotherapy applications, especially given the limitations in accessing such data from representatives of LINAC manufacturers who possess information about the LINAC components. Furthermore, the method proposed in this study can be a valuable tool for optimizing the use of the energy spectrum specific to any LINAC in radiotherapy services.

Acknowledgments

The authors express their gratitude to CNPq (Chamada Universal 427273/2016-1 and Chamada CNPq/MCTI/FNDCT Nº 18/2021 – Faixa B – Grupos Consolidados) for providing the hardware essential for conducting the simulations presented in this study. Additionally, the authors extend their appreciation to the Laboratory of Medical Physics at the Federal University of Health Sciences of Porto Alegre, the Center for Technology and Information of Ribeirão Preto CETI-RP, and Dosemed Soluções em Radioterapia for their invaluable data support, as well as to the Research Vice-Presidency of the University of Magdalena.

References

[1] S. Espenel, J.-C. Trone, and et al., Bull. Cancer **102**, 105 (2015).

[2] J. Wong, T. Schultheiss, and et al., *Advances in Radiation Oncology* (Springer, 2017).

[3] ICRU, *Prescribing, Recording and Reporting Photon Beam Therapy (Supplement to ICRU Report 50)*, Report 62 (U.S.A., 1999).

[4] I. Das, C. Cheng, and et al., Med. Phys. **35**, 4186 (2008).

[5] G. Kayal, M. Chauvin, and et al., Phys. Med. **85**, 24 (2021).

[6] J. Spiga, P. Pellicioli, and et al., Phys. Med. **66**, 45 (2019).

[7] D. Sarrut and et al., Med. Phys. **41**, 064301 (2014).

[8] A. Bennett and et al., Ann. Nucl. Energy **96**, 1 (2016).

[9] S. Taneja, L. Bartol, and et al., Int. J. Med. Phys. Clin. Eng. Radiat. Oncol. **9**, 186 (2020).

[10] F. Salvat and et al., *PENELOPE-2008: A Code System for Monte Carlo Simulation of Electron and Photon Transport*, NEA No. 6416 (OECD Nuclear Energy Agency, 2009).

[11] J. Sempau and et al., NIMB **207**, 107 (2003).

[12] B. Faddegon, J. Ramos-Méndez, and et al., Phys. Med. **72**, 114 (2020).

[13] J. Perl, J. Shin, and et al., Med. Phys. **39**, 6818 (2012).

[14] G. García Gómez-Tejedor and M. C. Fuss, eds., *Radiation Damage in Biomolecular Systems* (Springer, 2012).

[15] L. Brualla, M. Rodriguez, and et al., Radiat. Oncol. **14**, 6 (2019).

[16] L. de Sousa and et al., Braz. J. Radiat. Sci. **9**, 1639 (2019).

[17] A. Abou Jaoudé, ed., *The Monte Carlo Methods – Recent Advances, New Perspectives and Applications* (IntechOpen, London, United Kingdom, 2022).

[18] M. Alva-Sánchez and T. A. Pianoschi, Radiat. Phys. Chem. **167**, 108428 (2020).

[19] N. Souza Neto and et al., Braz. J. Radiat. Sci. **10**, 2049 (2022).

[20] D. Sheikh-Bagheri and D. Rogers, Med. Phys. **29**, 391 (2002).

[21] W. T. Jalbout and N. M. Spyrou, Phys. Med. Biol. **51**, 2211 (2006).

[22] J. Deng, S. B. Jiang, and et al., Phys. Med. Biol. **46**, 1429 (2001).

[23] J. P. O. Manrique, Nucl. Instrum. Methods Phys. Res. A **985**, 164684 (2021).

[24] J. Torres Díaz and et al., Phys. Med. **96**, 81 (2022).

[25] H. J. Choi, H. Park, and et al., Med. Phys. **46**, 3285 (2019).

[26] Z. Aboulbanine and K. Bahhous, Radiat. Phys. Chem. **201**, 110451 (2022).

[27] J. H. Wilches Visbal and A. M. Costa, Radiat. Phys. Chem. **162**, 31 (2019).

[28] J. Wei, G. A. Sandison, and et al., Med. Phys. **33**, 354 (2006).

[29] J. H. Wilches Visbal and P. Nicolucci, J. Appl. Res. Technol. **19**, 622 (2021).

[30] L. Zhengming and D. Jette, Phys. Med. Biol. **44**, N177 (1999).

[31] S. I. Kabanikhin, J. Inverse Ill-Posed Probl. **16**, 317 (2008).

[32] A.-M. Wazwaz, *Linear and Nonlinear Integral Equations: Methods and Applications* (Springer Berlin Heidelberg, 2011).

[33] L. Zhengming, Nucl. Instrum. Methods Phys. Res. A **255**, 152 (1987).

[34] P. C. Hansen, Inverse Problems **8**, 849 (1992).

[35] D. D. Bui and P. Nelson, Inverse Problems **8**, 821 (1992).

[36] Y. Xu, Y. Pei, and et al., Radiat. Phys. Chem. **50**, 1 (2016).

[37] P. C. Hansen, SIAM Rev. **34**, 561 (1992).

[38] J. Wilches-Visbal and D. Apaza-Veliz, Ing. y Competitividad **25**, e21112051 (2023).

[39] T. Schanze, Comput. Phys. Commun. **175**, 708 (2006).

[40] J. H. Wilches-Visbal, D. Apaza-Veliz, and et al., Uniciencia **36**, 1 (2022).

[41] V. Mariotti and et al., Radiat. Phys. Chem. **190**, 109782 (2022).

[42] D. Sheikh-Bagheri and D. W. O. Rogers, Med. Phys. **29**, 391 (2002).

[43] A. Baumgartner and et al., Appl. Radiat. Isot. **67**, 2007 (2009).

[44] A. Konefał, M. Cygan-Bakoniak, and et al., Radiat. Meas. **72**, 12 (2015).

[45] M. S. Alva-Sanchez and et al., Radiat. Meas. **176**, 107221 (2024).

[46] G. Ding, D. Rogers, and et al., *Energy spectra, angular spread and dose distributions of electron beams from various accelerators used in radiotherapy*, Tech. Rep. (Institute for National Measurement Standards, Ottawa, 1995).

[47] L. Apipunyasopon and et al., J. Radiat. Res. **54**, 374 (2013).

[48] S. Alashrah, S. Kandaiya, and et al., Radiat. Prot. Dosim. **162**, 338 (2014).

[49] M. Castro and et al., Radiat. Phys. Chem. **188**, 109748 (2021).

[50] J. Torres-Díaz and et al., Phys. Med. **96**, 81 (2022).

[51] B. Bednarz, C. Hancox, and et al., Phys. Med. Biol. **54**, 5271 (2009).

[52] H. Aamri, A. Fielding, and et al., Radiat. Phys. Chem. **178**, 109013 (2021).

[53] M. Assalmi and et al., Rep. Pract. Oncol. Radiother. **25**, 1001 (2020).

[54] G. Silva, V. Botelho, and et al., Applied Radiation and Isotopes **225**, 112087 (2025).